

# In Vitro and In Vivo Evaluation of Carboxymethyl Cellulose Scaffolds for Bone Tissue Engineering Applications

Ganesan Priya, Balaraman Madhan, Uttamchand Narendrakumar, Rayadurgam Venkata Suresh Kumar, and Inderchand Manjubala\*

Cite This: *ACS Omega* 2021, 6, 1246–1253

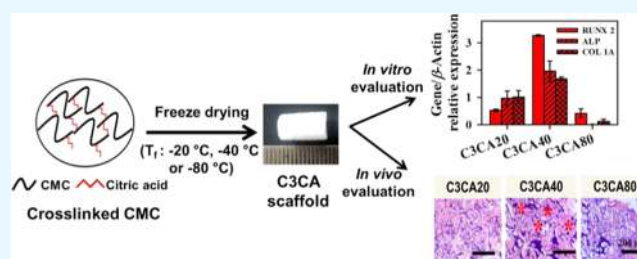
Read Online

ACCESS |

Metrics & More

Article Recommendations

**ABSTRACT:** The present study involves the development of citric acid-cross-linked carboxymethyl cellulose (C3CA) scaffolds by a freeze-drying process. Scaffolds were fabricated at different freezing temperatures of  $-20$ ,  $-40$ , or  $-80$  °C to investigate the influence of scaffold pore size on bone regeneration. All three scaffolds were porous in structure, and the pore size was measured to be  $74 \pm 4$ ,  $55 \pm 6$ , and  $46 \pm 5$   $\mu\text{m}$  for  $-20$ ,  $-40$ , and  $-80$  °C scaffolds. The pores were larger in scaffolds processed at  $-20$  °C compared to  $-40$  and  $-80$  °C, indicating the reduction in pore size of the scaffolds with a decrease in freezing temperature. The cytocompatibility, cell proliferation, and differentiation in C3CA scaffolds were assessed with the Saos-2 osteoblast cell line. These scaffolds supported the proliferation and differentiation of Saos-2 cells with significant matrix mineralization in scaffolds processed at  $-40$  °C. Subcutaneous implantation of C3CA scaffolds in the rat model was investigated for its ability of vascularization and new matrix tissue formation. The matrix formation was observed at the earliest of 14 days in the scaffolds when processed at  $-40$  °C while it was observed only after 28 days of implantation with the scaffolds processed at  $-20$  and  $-80$  °C. These results suggest that the citric acid-cross-linked CMC scaffolds processed at  $-40$  °C can be promising for bone tissue engineering application.



## INTRODUCTION

Bone has a self-healing capacity, but it is difficult to heal in critical size defects, which requires clinical intervention for its reunion and regeneration.<sup>1</sup> Three-dimensional (3D) scaffolds offer a promising platform for tissue regeneration that serves as a temporary support at the defective site and directs the cellular growth.<sup>1,2</sup> Polysaccharide and protein-based natural polymers such as chitosan, gelatin, alginate, collagen, cellulose, and their derivatives have been explored in various tissue engineering applications.<sup>3–7</sup> Carboxymethyl cellulose (CMC) is an anionic, water-soluble, biocompatible, and biodegradable polymer with excellent properties of high hydrophilicity, viscosity, defoaming, chelating, and antifouling abilities.<sup>3,8–11</sup> CMC hydrogels are well known for their swelling ability and sensitivity to pH and ionic strength variations; hence, it behaves as a smart polyelectrolyte.<sup>12</sup> The use of CMC has been widely established in pharmaceutical, drug and protein delivery, and wound healing applications.<sup>13–15</sup>

Being anionic, CMC has the ability to interact with chitosan and can form polyelectrolyte complexes for tissue engineering applications. CMC–chitosan membranes coated with nano-hydroxyapatite have shown improved morphology, stability, and bioactivity compared to pure chitosan membranes.<sup>16</sup> CMC is also incorporated in various polymer-based and ceramic-based composites and formulated as hydrogels, scaffolds,

injectable gels, and membranes for bone tissue engineering applications.<sup>17–20</sup> CMC hydrogels containing hydroxyapatite (HA) and  $\beta$ -tricalcium phosphate are reported to stimulate the mesenchymal stem cell differentiation toward osteogenic and odontogenic lineages.<sup>21–23</sup> CMC–hydroxyapatite nanocomposites are shown to have enhanced mechanical strength and have been proposed for load-bearing applications.<sup>24</sup> These reports suggested that CMC can be a suitable matrix for HA-based composites in bone tissue engineering due to the inherent capacities of CMC to undergo gelation by hydrogen bond and to induce  $\text{Ca}^{2+}$  chelation by its carboxylic groups.<sup>20,24–27</sup>

Though CMC has been used as promising scaffolds, a detailed investigation of their biological properties in terms of cytocompatibility, osteogenic differentiation, and mineralization is required to further establish their potential for bone tissue engineering applications. Citric acid (CA) has been used as a nontoxic cross-linker in the preparation of CMC-based

Received: September 16, 2020

Accepted: December 21, 2020

Published: January 4, 2021



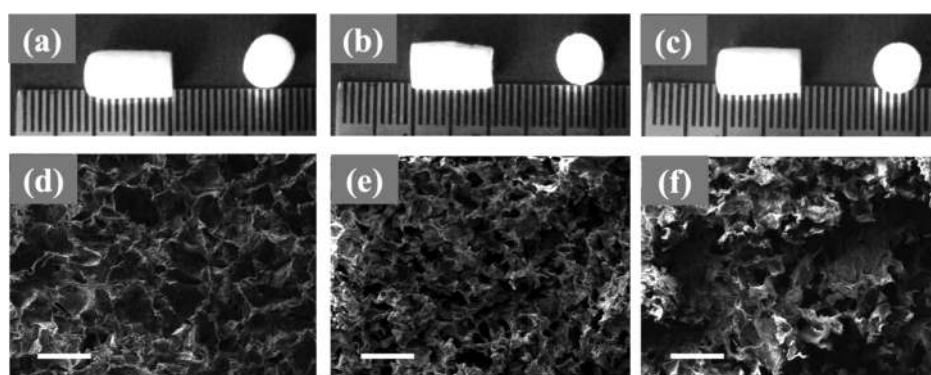


**Figure 1.** (a–c) Photographs and (d–f) cross-sectional morphologies of C3CA scaffolds processed at  $-20$ ,  $-40$ , and  $-80$  °C. All three scaffolds showed porous structures, and the pores were bigger in C3CA20 compared to those in C3CA40 and C3CA80. Scale bar:  $100\ \mu\text{m}$ .

hydrogels to enhance their biostability and superabsorbent behavior.<sup>10,15,21</sup> The present study involves the development of citric acid-cross-linked CMC scaffolds *via* freeze-drying process at three different freezing temperatures of  $-20$ ,  $-40$ , or  $-80$  °C. The freeze-drying process helps to fabricate highly porous scaffolds by permitting pore formation from the sublimation of ice crystals, and its key advantage is the possibility of fabricating scaffolds with varying pore properties.<sup>28</sup> The objective of this study is to evaluate the ability of the citric acid-cross-linked scaffolds to promote cell growth, differentiation, and mineralization in the presence of osteogenic induction. The new tissue formation by the CMC scaffolds in the subcutaneous implantation of the rat model was further investigated to determine their osteoinductive potential.

## RESULTS

**Scaffold Morphology and Porosity.** The photographs and the cross-sectional morphology of C3CA scaffolds processed at  $-20$ ,  $-40$ , and  $-80$  °C are shown in Figure 1, and their pore properties are listed in Table 1. All three

**Table 1. Pore Properties of C3CA Scaffolds Processed at  $-20$ ,  $-40$ , and  $-80$  °C<sup>a</sup>**

scaffolds	pore size ( $\mu\text{m}$ ) (mean $\pm$ SD)	total pore volume of pores $>2\ \mu\text{m}$ (cc/g)	surface area ( $\text{m}^2/\text{g}$ )	porosity (%)
C3CA20	$74 \pm 4$	0.016	9.66	$67 \pm 7$
C3CA40	$55 \pm 6$	0.008	3.79	$66 \pm 5$
C3CA80	$46 \pm 5$	ND	ND	$68 \pm 5$

<sup>a</sup>ND: not determined.

scaffolds showed porous structures with interconnected pores (Figure 1d–f). The pore size of the scaffolds was measured to be  $74 \pm 4$ ,  $55 \pm 6$ , and  $46 \pm 5\ \mu\text{m}$  at  $-20$ ,  $-40$ , and  $-80$  °C, respectively. The decrease in freezing temperature from  $-20$  to  $-80$  °C has resulted in the reduction of pore size of the scaffolds. The surface area and pore volume of C3CA20 are  $9.66\ \text{m}^2/\text{g}$  and  $0.016\ \text{cc/g}$ , respectively, while C3CA40 showed the corresponding values of  $3.79\ \text{m}^2/\text{g}$  and  $0.008\ \text{cc/g}$ . The surface area and pore volume of C3CA80 were not determined due to the presence of smaller pores that made it difficult to calculate their pore properties. The scaffolds had porosities of  $67 \pm 7$ ,  $66 \pm 5$ , and  $68 \pm 5\%$  at  $-20$ ,  $-40$ , and  $-80$  °C, indicating that the change in freezing temperature has not affected the porosity of the scaffolds.

**Swelling Property.** The absorption of phosphate-buffered saline (PBS) was found to be spontaneous in all of the scaffolds, and the swelling ratios of C3CA20, C3CA40, and C3CA80 were found to be  $644 \pm 41$ ,  $640 \pm 20$ , and  $548 \pm 42\%$ , respectively. It can be inferred that the swelling ratio is lower in C3CA80 than in C3CA20 and C3CA40 scaffolds. It is due to the presence of smaller pores in C3CA80 that rendered less uptake of PBS into the pores of the scaffolds.

**Cell Proliferation and Differentiation.** The proliferation of Saos-2 cells in C3CA scaffolds after 4, 7, and 14 days of culture is shown in Figure 2a. The obtained absorbance value indicates the metabolic activity of proliferating cells. The increase in absorbance from day 4 to 14 indicates the consistent proliferation of cells with time. On day 14, the cell proliferation in C3CA20 is significantly higher than in C3CA40 and C3CA80 scaffolds. The alkaline phosphatase

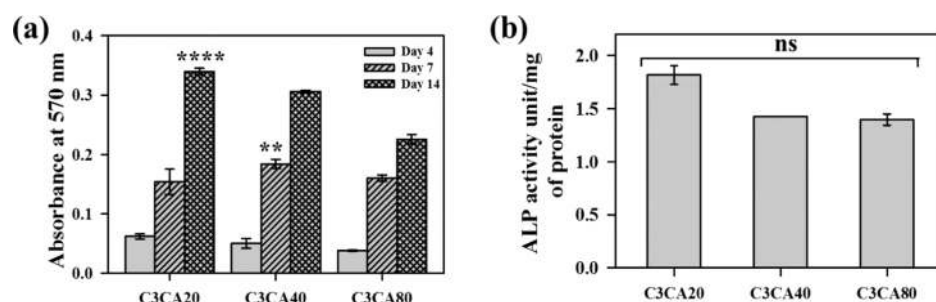


**Figure 2.** (a) Proliferation of Saos-2 cells after 4, 7, and 14 days of culture in C3CA scaffolds (processed at  $-20$ ,  $-40$ , and  $-80$  °C), measured by 3-(4,5-dimethylthiazol-2-yl)-2,5-diphenyl tetrazolium (MTT) assay (no significant difference among samples on day 4;  $**p < 0.01$  for comparison between C3CA40 vs C3CA20 and C3CA80 on day 7;  $****p < 0.0001$  for comparison between C3CA20 vs C3CA40, and C3CA80 on day 14). (b) ALP activity of the cells after 4 days of culture in C3CA scaffolds (ns represents no significant difference among samples).

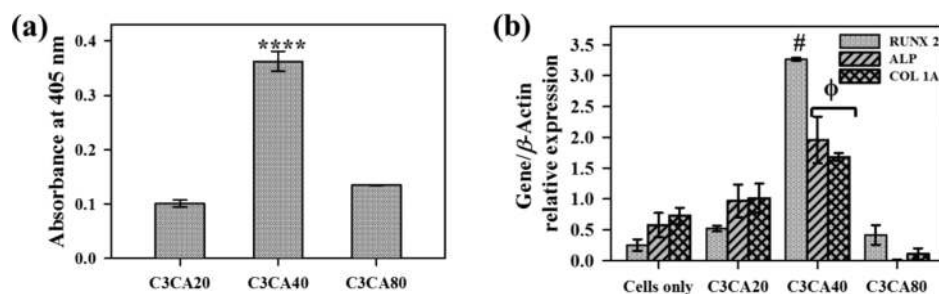


**Figure 3.** (a) Quantification of matrix mineralization after 21 days of cell culture in C3CA scaffolds (\*\*\*\* $p < 0.0001$  for comparison between C3CA40 vs C3CA20 and C3CA80). (b) Relative gene expressions of RUNX 2, ALP, and COL 1A after 4 days of culture in C3CA scaffolds ( $\#p < 0.001$  and  $\phi p < 0.01$  for comparison between C3CA40 and C3CA80). C3CA40 can preferentially promote cell differentiation and mineralization than C3CA20 and C3CA80 as indicated by its significant mineralization and gene upregulation.

(ALP) expression by the Saos-2 cells after 4 days of culture in C3CA scaffolds is shown in Figure 2b. All three scaffolds showed a considerable amount of ALP activity (1.4–1.8 unit/mg of protein) with no significant difference among the C3CA scaffolds.

**Mineralization and Gene Expression.** The mineralization of the cell matrix by Saos-2 cells after 21 days of culture in C3CA scaffolds is shown in Figure 3a. The cells in C3CA40 showed a significant amount of matrix mineralization compared to the C3CA20 and C3CA80 scaffolds analyzed by quantitative Alizarin Red S (ARS) assay. The mRNA expression of osteoblast-specific genes by the cells after 4 days of culture in C3CA scaffolds is shown in Figure 3b. Interestingly, C3CA40 showed significantly higher expressions of runt-related transcription factor 2 (RUNX 2), collagen type-1 (COL 1A), and ALP genes compared to C3CA20 and C3CA80 scaffolds. These results suggest that C3CA40 can preferentially promote the differentiation and mineralization of Saos-2 cells than C3CA20 and C3CA80 scaffolds.

**Subcutaneous Implantation Analysis.** The hematoxylin and eosin (H&E)-stained images of the subcutaneously implanted C3CA scaffolds (processed at  $-20$ ,  $-40$ , and  $-80$  °C) after predetermined time intervals are shown in Figure 4. At 3 days post-implantation, all of the C3CA implants showed acute to moderate inflammatory response, which is accompanied by the infiltration of neutrophils and red blood cells (RBCs). The immune response in the implants was reduced after 7 days of implantation. At 14 days post-implantation, C3CA40 showed the presence of blood capillaries (indicated by red arrows, Figure 4) and pink-colored matrix tissues (indicated by red asterisks, Figure 4), which indicate the vascularization and new tissue formation in the implant. In the case of C3CA80, only the blood capillaries were observed on day 14 while C3CA20 showed the presence of blood capillaries only after 21 days of implantation. All of the implants showed the infiltration of fibroblast cells by 21 days post-implantation (indicated by yellow arrows, Figure 4). These fibroblast cells will further help in the synthesis of extracellular matrices in the implant. C3CA20 and C3CA80 showed the new tissue formation only after 28 days of implantation, which is quite delayed compared to C3CA40 scaffolds. The reduction of the scaffold material and the replacement of fibrous tissues can also be observed after 28 days of implantation. The penetration of large blood capillaries from the peripheral tissues (Pt) was observed in the implants at 35 days post-implantation (indicated by red arrows, Figure 4).

The Masson's trichrome-stained images of C3CA implant sections after 28 and 35 days of implantation are shown in

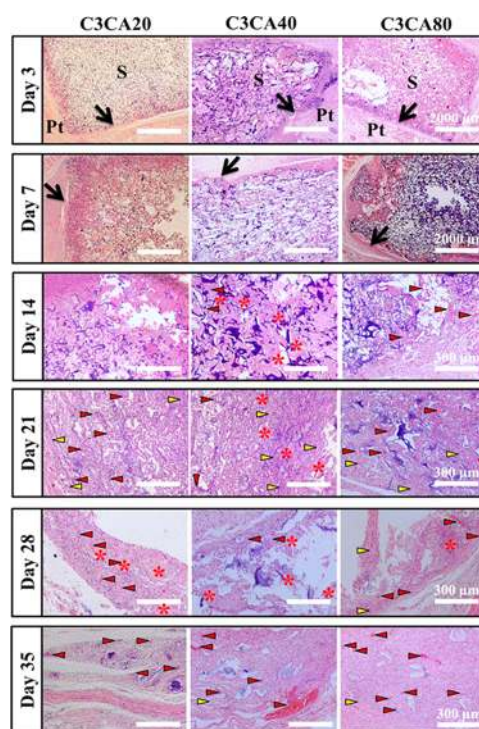


**Figure 4.** H&E staining of the C3CA implant sections after defined time intervals. Cellular infiltration into the implants is indicated by black arrows on days 3 and 7. C3CA40 showed blood vessel and new matrix formation on day 14, while C3CA20 and C3CA80 showed matrix formation only after 28 days of implantation. Pt, peripheral tissue; S, scaffold; red asterisk, new matrix formation; red arrows, blood vessels; yellow arrows, fibrous tissue in-growth.

**Figure 5.** The collagen deposition in the implants can be identified as green-colored fibrous matrices. All three implants showed the positive staining of collagen deposition after 28 days of implantation (indicated by yellow arrows, Figure 5). On day 35, the cross sections of many blood vessels were observed in all three implant sections in addition to collagen staining (as indicated by red arrows, Figure 5). This indicated the matrix tissue formation and rich blood supply in the implants.

The immunohistochemical staining of CD31 and osteocalcin markers in the C3CA implant sections at 35 days post-implantation is shown in Figure 6. All three implants showed positive staining of CD31 marker, indicating the presence of endothelial cells (indicated by red arrows). This further confirms the vascularization in the implants. All three implants

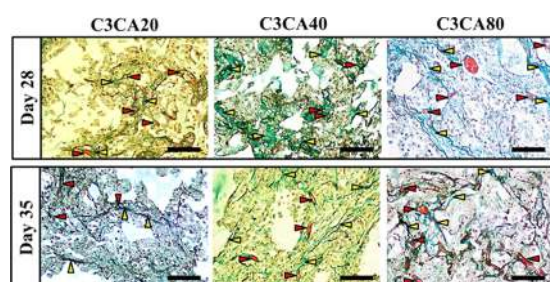


**Figure 5.** Masson's trichrome staining of C3CA implant sections after 28 and 35 days of implantation. Red arrows, blood vessels; yellow arrows, collagen deposition. Scale bar: 100  $\mu\text{m}$ .

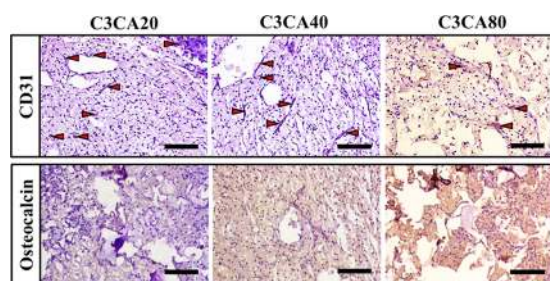


**Figure 6.** Immunohistochemical staining of C3CA implant sections with anti-CD31 and anti-osteocalcin after 35 days of implantation. Positive staining of CD31 confirmed the vascularization in the implants. The presence of mild staining of osteocalcin-positive cells indicates the unconfined cells to osteoblastic lineage. The red arrows indicate blood vessels. Scale bar: 100  $\mu\text{m}$ .

showed mild staining for the presence of osteocalcin-positive cells, indicating that the cells are yet to differentiate into the osteoblastic lineage.

The scanning electron microscopic images of the implants after 35 days of implantation are shown in Figure 7. All three

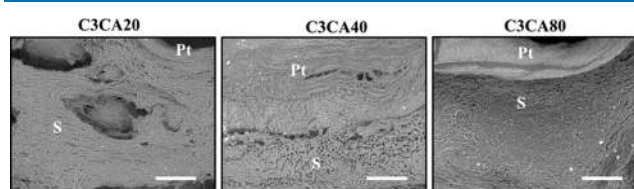


**Figure 7.** Scanning electron microscopic images of C3CA implants after 35 days of implantation. Fibrous tissue in-growths into the pore spaces of implants as indicated with no apparent difference between peripheral tissues (Pt) and implant material (S). Scale bar: 500  $\mu\text{m}$ .

implants showed significant fibrous tissue in-growths into their pore spaces as there was no apparent difference between the implant and the peripheral tissues. The large region without any tissue formation in the center of C3CA20 is due to the presence of a pore in the scaffold that was formed during the fabrication process. Because of the larger pore size, penetration of tissues was not observed or it may take longer time than 35 days of implantation for tissue penetration into such bigger pores of the scaffolds.

## DISCUSSION

In tissue engineering, effective bone regeneration can be achieved by involving the use of osteogenic, osteoconductive, and osteoinductive scaffolds. CMC has been used for bone tissue engineering in recent years, in various forms like

injectable gels, hydrogels, composites, films, and scaffolds.<sup>17–20</sup> However, the abilities of *in vitro* osteogenic differentiation and *in vivo* tissue formation of CMC were not widely explored. In this study, CMC scaffolds cross-linked with citric acid and processed at freezing temperatures of  $-20$ ,  $-40$ , and  $-80$   $^{\circ}\text{C}$  were evaluated for their osteogenic and new tissue formation abilities. Unlike other cross-linkers of CMC such as epichlorohydrin, glutaraldehyde, and genipin, citric acid is a natural polycarboxylic acid that is biocompatible, biodegradable, and an important metabolite in the body; hence, it is safe to be used in medical applications.<sup>8,29–33</sup>

Scaffolds used in tissue engineering should possess interconnected porous structure and high porosity to provide scope for cell adhesion, proliferation, and migration of invading cells into scaffolds.<sup>34</sup> As observed from the microscopic images, C3CA scaffolds were porous in structure with interconnected pores. The pore formation in the freeze-dried scaffolds can be tailored by controlling the freezing rate during the fabrication process.<sup>28</sup> Increasing the cooling rate of the samples during the freezing process leads to a rapid formation of ice crystals, which are the negative replicas of the pores.<sup>28,35</sup> In the present study, decreasing the freezing temperature from  $-20$  to  $-80$   $^{\circ}\text{C}$  during the fabrication process reduced the pore size in C3CA scaffolds. However, changing the freezing temperature did not affect the porosity of the scaffolds. The obtained results are in agreement with the earlier results published by Guex et al. and Haugh et al. who reported reduced pore size at increasing freezing rate.<sup>28,36</sup> Swelling ability is crucial for the scaffolds to facilitate cell infiltration in a three-dimensional manner, during *in vitro* and *in vivo* tissue formation.<sup>37</sup> Further, it helps us to promote the supply of nutrients and oxygen to the cells that are present in the inner regions of the scaffolds. All three C3CA scaffolds showed good swelling ability and were stable in PBS for more than 24 h; thus, these scaffolds are favorable for tissue engineering applications.

The cytocompatibility of C3CA scaffolds processed at different freezing temperatures was studied with the 3D culture of Saos-2 cells. Cell lines such as MC3T3-E1, UMR-106, and Saos-2 are osteogenic precursors that can differentiate and mineralize the bone matrix similar to native osteoblasts. Hence, these cell lines are commonly used in the osteogenic differentiation studies of scaffolds for bone regeneration applications.<sup>38–40</sup> Saos-2 cells are human-derived osteoblast cells, and therefore, it is more advantageous to use those cells in the *in vitro* evaluation of scaffolds. All three C3CA scaffolds facilitated the proliferation of Saos-2 cells as observed by increased metabolic activity on day 14. This suggests that the C3CA scaffolds can be a favorable substrate for cell adhesion and proliferation, thus indicating their cytocompatibility.

The differentiation phase of osteogenic cells can be identified in a variety of ways, such as alkaline phosphatase activity, matrix mineralization, and mRNA expression of osteogenic genes.<sup>36</sup> ALP activity of the cells increases the local concentration of free phosphates and initiates the active transport of calcium and phosphate across their cell membrane.<sup>21</sup> The osteoblast cells attain maximum ALP activity during the matrix maturation phase, and their expression is downregulated once the mineralization begins.<sup>41,42</sup> The ALP activity and the gene expression results in the present study suggest that the Saos-2 cells are in the early phase of osteogenic differentiation. RUNX 2 is a marker for early osteogenic differentiation, and it further induces the expression of ALP and Col 1A for matrix synthesis and mineralization.<sup>43</sup>

The significant upregulation of all three genes with prominent mineralization of cell matrices in C3CA40 indicates that the Saos-2 cells are preferentially mineralizing its matrix in C3CA40 compared to C3CA20 and C3CA80 scaffolds. Though the bigger pores of C3CA20 provided space for a large number of cells to infiltrate and proliferate, it did not contribute to the mineralization of cell matrices as expected. On the other hand, the pore size of C3CA40 facilitated the initial proliferation as well as mineralization process in prolonged culture time. The pores of C3CA80 are too small for the cells to effectively undergo proliferation and mineralization. Thus, it can be inferred that the pore morphology of  $-40\text{ }^{\circ}\text{C}$ -processed scaffolds was favorable for the cells to undergo early osteogenesis.

The *in vivo* osteoinductive potential of C3CA scaffolds can be evaluated by their bone-forming ability in an ectopic site where the osteogenic cues are limited. Cell infiltration, vascularization, fibrous tissue in-growth, and matrix tissue formation followed by their mineralization are the sequential parameters that must reach a dynamic balance for successful bone induction.<sup>44</sup> Besides, these parameters help us to evaluate the biocompatibility, immune response, and *in vivo* stability of the scaffolds when implanted subcutaneously in the animals.<sup>45,46</sup> In the present study, the scaffolds were implanted subcutaneously in the rats and their immune response, cellular infiltration, and matrix deposition were evaluated. The neutrophils that are seen in the initial days of implantation of scaffolds are mainly due to the immune responses for foreign material and surgical procedures.

Vascularization in the implants is another important factor for tissue formation.<sup>44</sup> The presence of blood vessels in the implants was observed in the H&E and Masson's trichrome-stained implant sections. This was further confirmed with the positive staining of CD31, a highly sensitive and specific protein marker of endothelial cells.<sup>47</sup> These results confirm the vascularization in the implants, and this can continuously supply nutrients and oxygen to the cells found interior in the implants. The active fibroblasts in the implants at 21 days post-implantation contribute to the synthesis of collagen and other extracellular matrix proteins. The collagen deposition by the cells further promotes the formation of the unmineralized organic matrix osteoid that contains growth factors, cytokines, and other proteins for bone formation. The new matrix formation was observed as early as 14 days in C3CA40 ( $55 \pm 6\ \mu\text{m}$ ), accompanied by organized collagen networks by 35 days of implantation. The smaller pores in C3CA80 ( $46 \pm 5\ \mu\text{m}$ ) supported early vascularization similar to C3CA40 but could not form the matrix tissue due to limited pore space. The blood vessel and matrix formation in C3CA20 ( $74 \pm 4\ \mu\text{m}$ ) is quite delayed due to its larger pores, indicating that it requires a longer time for osteoinduction.

The pore size of the C3CA scaffolds in the present study was lower than the pore size (minimum  $100\ \mu\text{m}$ ) suggested for optimal bone in-growth, osteoconduction, and osteoinduction.<sup>28,48</sup> However, all three C3CA scaffolds facilitated vascularization, collagen deposition, and new matrix formation at the earliest of implantation compared to decellularized-cellulose (8 weeks), bacterial cellulose (4 weeks) scaffolds, and tricalcium phosphate–calcium silicate composites (8 weeks) reported for bone regeneration.<sup>46,49,50</sup> The most striking difference is the early vascularization and new matrix formation in C3CA40 compared to C3CA20 and C3CA80 scaffolds. Apart from this, the vascularization and matrix tissue formation

are exclusively achieved from the intrinsic osteoinductive effect of CMC. It is also expected that the addition of osteoinductive stimuli like calcium phosphates, bone morphogenetic proteins, stem cells, osteoblasts, cytokines, growth factors, *etc.* would enhance the matrix tissue formation, and thereby, it can contribute to new bone formation.<sup>46</sup>

## CONCLUSIONS

In this study, citric acid-cross-linked CMC scaffolds processed at three freezing temperatures of  $-20$ ,  $-40$ , and  $-80\text{ }^{\circ}\text{C}$  were fabricated by the freeze-drying method. The scaffolds facilitated the proliferation of Saos-2 cells, as well as permitted the differentiation and mineralization of cell matrices *in vitro*. Subcutaneous implantation of citric acid-cross-linked CMC scaffolds in a rat model showed vascularization and new matrix formation in the implants. The C3CA scaffolds processed at  $-40\text{ }^{\circ}\text{C}$  with a pore size of  $55 \pm 6\ \mu\text{m}$  can indeed enhance the differentiation and mineralization of Saos-2 cells *in vitro* and new matrix formation *in vivo*. These results clearly demonstrated the osteogenic and osteoinductive potential of CMC scaffolds cross-linked with citric acid.

## MATERIALS AND METHODS

**Materials.** Sodium carboxymethyl cellulose (viscosity, 1500–3000 cP) and citric acid were obtained from HiMedia, India, and used without further processing. Cell culture media ( $\alpha$ -modified Eagle's medium,  $\alpha$ -MEM), fetal calf serum (FCS), penicillin, and streptomycin were purchased from Gibco. Other chemicals used in the experiments were all of the analytical grades.

**Fabrication of Scaffolds.** CMC solution (2.5 wt %) was prepared in double-distilled water under continuous stirring to obtain a homogeneous viscous solution and mixed with citric acid (CA, 2.0 wt % dissolved in  $100\ \mu\text{L}$  of distilled water) for about 5–10 min to get a cross-linked CMC solution (named as C3CA). All of the solutions were cast in polystyrene molds of size 6.5 mm diameter  $\times$  10.5 mm height and processed at freezing temperatures of  $-20$ ,  $-40$ , and  $-80\text{ }^{\circ}\text{C}$  for 36 h (named as C3CA20, C3CA40, and C3CA80). It is followed by freeze-drying in a lyophilizer (LYO0555, Delvac, India) at a temperature of  $-40\text{ }^{\circ}\text{C}$  ( $\sim 0.09\ \text{mmHg}$ ) for 48 h.

**Morphological Analysis and Porosity Measurement.** Cylindrical C3CA scaffolds (6 mm diameter  $\times$  10 mm height) were cut into halves (*i.e.*, 5 mm from the bottom), and the morphology at the cross section was examined using a scanning electron microscope (Carl Zeiss, EVO 18 SEM), operated at an accelerating voltage of 10 kV and a working distance of 10 mm. The surface was sputter-coated with gold palladium (Quorum sputter-coater). The pore size of the scaffolds was measured using ImageJ software (1.49v, NIH Image) in the manual mode. At least 20 pores were assessed at one SEM image (magnification, 400 $\times$ ) for each scaffold composition. The randomly selected pores were analyzed for the long pore axis, and an average of 20 pores were determined. The pore volume and surface area of the scaffolds were calculated by the Brunauer–Emmett–Teller (BET) method in a pore size analyzer (QUADRASORB SI, Quantachrome Instruments, Germany).

The porosity of the scaffolds was measured by an ethanol displacement method, as reported by Kim *et al.*<sup>34</sup> The initial weight ( $W_i$ ) of the scaffolds was measured, and the scaffolds were immersed in ethanol for 1 h at  $37\text{ }^{\circ}\text{C}$  to fill the pores with

ethanol diffusion. Then, the scaffolds were removed and the weight ( $W_f$ ) was measured. The percentage porosity of the scaffolds is calculated using eq 1, where  $\rho$  is the density of ethanol and  $V_s$  is the full volume of the scaffold.

$$\text{porosity (\%)} = ((W_f - W_i)/(\rho \times V_s)) \times 100 \quad (1)$$

**Swelling Property.** The swelling ratio of the scaffolds was measured by immersing in phosphate-buffered saline (PBS, pH 7.4) at 37 °C. The initial dry weight ( $W_i$ ) of the scaffolds (6 mm diameter  $\times$  3 mm height) was measured. After 24 h of immersion in PBS, the weight of the wet scaffolds was noted ( $W_f$ ). The swelling ratio of the scaffolds was calculated using eq 2.

$$\text{swelling ratio (\%)} = \frac{W_f - W_i}{W_i} \times 100 \quad (2)$$

**Cell Culture and Seeding.** Saos-2 cells were obtained from National Centre for Cell Science, Pune, India, and cultured in  $\alpha$ -MEM containing 10% FCS and 2% penicillin–streptomycin. The cells were maintained in a humidified incubator at 37 °C and 5% carbon dioxide. C3CA scaffolds (6 mm diameter  $\times$  1 mm height) were seeded with 10  $\mu$ L of the cell suspension at  $5 \times 10^6$ /mL concentration and incubated at 37 °C for 2 h to allow cell adhesion. After 24 h, the medium was changed to an osteogenic medium that contained osteogenic factors like  $\beta$ -glycerophosphate (10 mM), L-ascorbic acid-2-phosphate (50  $\mu$ g/mL), and dexamethasone (100 nM) in  $\alpha$ -MEM. The cell-seeded scaffolds were maintained under the standard culture conditions by changing the osteogenic media twice per week. For the assessment of cell proliferation, the cells were maintained in the basal medium, whereas the cells cultured in the osteogenic medium were used in the assessment of differentiation, mineralization, and gene expression studies.

**Cell Proliferation and Differentiation.** The proliferation of Saos-2 cells on C3CA scaffolds was measured by 3-(4,5-dimethylthiazol-2-yl)-2,5-diphenyl tetrazolium (MTT) assay after 4, 7, and 14 days of culture. The metabolically active cells present in the scaffolds reduce the MTT dye into insoluble purple crystals, which were subsequently dissolved in dimethyl sulfoxide. The absorbance of the purple-colored solution was measured at 570 nm using an enzyme-linked immunosorbent assay (ELISA) microplate reader (Synergy HT, BioTek Instruments, Inc.).

Alkaline phosphatase (ALP) is an early marker for differentiation toward osteogenic phenotype. The ALP activity of the Saos-2 cells was assessed by *p*-nitrophenyl phosphate (*p*-NPP) assay after 4 days of culture. The cells were lysed with the radio-immunoprecipitation assay (RIPA) buffer for the release of intracellular ALP enzymes, and the *p*-NPP substrate was added to the lysate for the formation of *p*-nitrophenol whose absorbance was measured at 405 nm. The ALP activity was normalized to the total protein content of the cells and is expressed as the activity unit per milligram of protein.

**Mineralization and Osteogenic Gene Expression.** The matrix mineralization in C3CA scaffolds by the Saos-2 cells was assessed by Alizarin Red S (ARS) staining after 21 days of culture. The cell-seeded scaffolds were stained with ARS (2.0 wt %) for 2 min, and after the removal of excess stain, the scaffolds were destained with acetic acid (10% v/v). The absorbance of the destained solution was measured at 405 nm.

The osteogenic differentiation of the Saos-2 cells was determined by analyzing mRNA expression of runt-related transcription factor 2 (RUNX 2), alkaline phosphatase (ALP), and collagen type-1 (COL 1A) after 4 days of culture. The total RNA present in the cultured cells was isolated by the TRIzol method, and about 2.5  $\mu$ g of RNA was reverse-transcribed to complementary DNA (cDNA) using a high-capacity RNA-to-cDNA kit (Thermo Fisher Scientific). Quantitative real-time polymerase chain reaction (qRT-PCR) was carried out using TaqMan Universal PCR master mix and gene expression assays using StepOnePlus real-time PCR system (Applied Biosystems). The relative expressions of each target gene were normalized against CT values of the housekeeping gene ( $\beta$ -actin) by the  $2^{-\text{ddCT}}$  method, where the ddCT values were calculated using eq 3. The gene expression in the cells without scaffolds (cells only) was also analyzed to compare the expression pattern with the cell-seeded scaffolds. The data are reported as relative gene expression in osteogenic media (Ost) compared to standard culture media as the control.

$$\text{ddCT} = (\text{CT}^{\text{target}} - \text{CT}^{\text{actin}})_{\text{OST}} - (\text{CT}^{\text{target}} - \text{CT}^{\text{actin}})_{\text{CONTROL}} \quad (3)$$

**Subcutaneous Implantation of Scaffolds.** The ability of C3CA scaffolds (processed at  $-20$ ,  $-40$ , and  $-80$  °C) to facilitate new tissue formation was evaluated by its subcutaneous implantation in a rat model. All of the experimental procedures were approved by the Institutional Animal Ethics Committee of Vellore Institute of Technology, Tamil Nadu (VIT/IAEC/12). A total of 30 male Albino Wistar rats (4–5 weeks old; weight, 180–220 g) were used in this study. The rats were anesthetized with an intramuscular injection of a mixture of ketamine (10 mg/kg body weight) and xylazine (10 mg/kg body weight). After shaving the skin, longitudinal incisions (1 cm) were made at three different regions in the dorsum of each rat to create subcutaneous pockets. All three scaffolds (6 mm diameter  $\times$  10 mm height) were inserted on either side of the same animal, and the incisions were sutured and antisepticated. After 24 h, a dose of antibiotics (sulfadoxine and trimethoprim at a 5:1 ratio, 15 mg/kg body weight) was given to the rats. At 3, 7, 14, 21, 28, and 35 days post-implantation, the animals were euthanized by CO<sub>2</sub> inhalation and the implants with the surrounding tissues were excised and fixed in 10% phosphate-buffered formalin for histological analysis. Five animals per time point were used for the analysis. The implants excised at 35 days post-implantation were fixed in 2.5% glutaraldehyde for scanning electron microscopic analysis.

**Histological Staining.** Formalin-fixed implants were dehydrated, embedded in paraffin wax, and serial longitudinal sections of 5  $\mu$ m thickness were made using a microtome (Leica, 2125RT). The implant sections were stained with hematoxylin–eosin (H&E) to elucidate histological features. Masson's trichrome counter-staining with light-green SF of the implant sections was used to identify the collagen deposition in the implant sections. Immunohistochemical staining of CD31 and osteocalcin markers in the implant sections was performed using IHC staining kit (PathnSitu Biotechnologies Pvt Ltd., India). A bright-field optical microscope was used to visualize the implant sections at 10 $\times$  and 20 $\times$  magnifications (Olympus BX51).

**Statistical Analysis.** All quantitative data are reported as mean  $\pm$  standard deviation (SD) and analyzed statistically by one-way analysis of variance (ANOVA) with Tukey's post hoc test ( $p < 0.05$ ) using GraphPad Prism 6.0 (GraphPad Software, Inc.). All of the data with  $p \leq 0.05$  are considered statistically significant.

## AUTHOR INFORMATION

### Corresponding Author

**Inderchand Manjubala** – Department of Biosciences, School of Bio Sciences and Technology, Vellore Institute of Technology, Vellore 632014, India; [orcid.org/0000-0003-4873-2377](https://orcid.org/0000-0003-4873-2377); Phone: +91-416-2202513; Email: [i.manjubala@vit.ac.in](mailto:i.manjubala@vit.ac.in); Fax: +91-416-224 3092

### Authors

**Ganesan Priya** – Department of Biosciences, School of Bio Sciences and Technology, Vellore Institute of Technology, Vellore 632014, India

**Balaraman Madhan** – Centre for Academic and Research Excellence (CARE), CSIR-CLRI, Chennai 600020, India

**Uttamchand Narendrakumar** – Department of Manufacturing Engineering, School of Mechanical Engineering, Vellore Institute of Technology, Vellore 632014, India

**Rayadurgam Venkata Suresh Kumar** – Department of Surgery and Radiology, Sri Venkateshwara Veterinary University, Tirupati S17502, India

Complete contact information is available at:

<https://pubs.acs.org/10.1021/acsomega.0c04551>

### Author Contributions

I.M. formulated the concept, idea, and methodology; analyzed the data; discussed; and contributed to framing and writing the manuscript. The experiments were performed by G.P. Some experiments were conducted and analyzed by B.M. The animal experiments were supervised by R.V.S.K. Analysis and discussion of results and manuscript framing were done by U.N. The manuscript was written through contributions of all authors. All authors have given approval to the final version of the manuscript.

### Notes

The authors declare no competing financial interest.

## ACKNOWLEDGMENTS

G.P. and I.M. are grateful to Department of Science and Technology, Science and Engineering Research Board, Government of India (SB/FTP/ETA-0119/2013), and VIT SEED GRANT (RGEMS) and SBST School fund, Vellore Institute of Technology, for the financial support. The authors acknowledge Vellore Institute of Technology for scanning electron microscopy facility (DST-FIST cum VIT-funded). G.P. and I.M. thank Arun, CSIR-Central Leather Research Institute for electron microscopic imaging of implants.

## REFERENCES

(1) Poh, P. S.; Hutmacher, D. W.; Holzapfel, B. M.; Solanki, A. K.; Stevens, M. M.; Woodruff, M. A. In vitro and in vivo bone formation potential of surface calcium phosphate-coated polycaprolactone and polycaprolactone/bioactive glass composite scaffolds. *Acta Biomater.* **2016**, *30*, 319–333.

(2) Manjubala, I.; Scheler, S.; Bossert, J.; Jandt, K. D. Mineralisation of chitosan scaffolds with nano-apatite formation by double diffusion technique. *Acta Biomater.* **2006**, *2*, 75–84.

(3) Singh, B.; Panda, N.; Mund, R.; Pramanik, K. Carboxymethyl cellulose enables silk fibroin nanofibrous scaffold with enhanced biomimetic potential for bone tissue engineering application. *Carbohydr. Polym.* **2016**, *151*, 335–347.

(4) Shi, Q.; Li, Y.; Sun, J.; Zhang, H.; Chen, L.; Chen, B.; Yang, H.; Wang, Z. The osteogenesis of bacterial cellulose scaffold loaded with bone morphogenetic protein-2. *Biomaterials* **2012**, *33*, 6644–6649.

(5) Li, Z.; Ramay, H. R.; Hauch, K. D.; Xiao, D.; Zhang, M. Chitosan–alginate hybrid scaffolds for bone tissue engineering. *Biomaterials* **2005**, *26*, 3919–3928.

(6) Schneider, R. K.; Puellen, A.; Kramann, R.; Raupach, K.; Bornemann, J.; Knuechel, R.; Pérez-Bouza, A.; Neuss, S. The osteogenic differentiation of adult bone marrow and perinatal umbilical mesenchymal stem cells and matrix remodelling in three-dimensional collagen scaffolds. *Biomaterials* **2010**, *31*, 467–480.

(7) Zhang, F.; He, C.; Cao, L.; Feng, W.; Wang, H.; Mo, X.; Wang, J. Fabrication of gelatin–hyaluronic acid hybrid scaffolds with tunable porous structures for soft tissue engineering. *Int. J. Biol. Macromol.* **2011**, *48*, 474–481.

(8) Akar, E.; Altınışık, A.; Seki, Y. Preparation of pH-and ionic-strength responsive biodegradable fumaric acid crosslinked carboxymethyl cellulose. *Carbohydr. Polym.* **2012**, *90*, 1634–1641.

(9) Dilaver, M.; Yurdakoc, K. Fumaric acid cross-linked carboxymethylcellulose/poly (vinyl alcohol) hydrogels. *Polym. Bull.* **2016**, *73*, 2661–2675.

(10) Gorgieva, S.; Kokol, V. Synthesis and application of new temperature-responsive hydrogels based on carboxymethyl and hydroxyethyl cellulose derivatives for the functional finishing of cotton knitwear. *Carbohydr. Polym.* **2011**, *85*, 664–673.

(11) Yadollahi, M.; Namazi, H.; Barkhordari, S. Preparation and properties of carboxymethyl cellulose/layered double hydroxide bionanocomposite films. *Carbohydr. Polym.* **2014**, *108*, 83–90.

(12) Sannino, A.; Demitri, C.; Madaghiele, M. Biodegradable cellulose-based hydrogels: design and applications. *Materials* **2009**, *2*, 353–373.

(13) Jeong, D.; Joo, S.-W.; Hu, Y.; Shinde, V. V.; Cho, E.; Jung, S. Carboxymethyl cellulose-based superabsorbent hydrogels containing carboxymehtyl  $\beta$ -cyclodextrin for enhanced mechanical strength and effective drug delivery. *Eur. Polym. J.* **2018**, *105*, 17–25.

(14) Basu, P.; Narendrakumar, U.; Arunachalam, R.; Devi, S.; Manjubala, I. Characterization and Evaluation of Carboxymethyl Cellulose-Based Films for Healing of Full-Thickness Wounds in Normal and Diabetic Rats. *ACS Omega* **2018**, *3*, 12622–12632.

(15) Zheng, W. J.; Gao, J.; Wei, Z.; Zhou, J.; Chen, Y. M. Facile fabrication of self-healing carboxymethyl cellulose hydrogels. *Eur. Polym. J.* **2015**, *72*, 514–522.

(16) Liuyun, J.; Yubao, L.; Li, Z.; Jianguo, L. Preparation and properties of a novel bone repair composite: nano-hydroxyapatite/chitosan/carboxymethyl cellulose. *J. Mater. Sci.: Mater. Med.* **2008**, *19*, 981–987.

(17) Vimalraj, S.; Saravanan, S.; Vairamani, M.; Gopalakrishnan, C.; Sastry, T.; Selvamurugan, N. A Combinatorial effect of carboxymethyl cellulose based scaffold and microRNA-15b on osteoblast differentiation. *Int. J. Biol. Macromol.* **2016**, *93*, 1457–1464.

(18) Sainitya, R.; Sriram, M.; Kalyanaraman, V.; Dhivya, S.; Saravanan, S.; Vairamani, M.; Sastry, T.; Selvamurugan, N. Scaffolds containing chitosan/carboxymethyl cellulose/mesoporous wollastonite for bone tissue engineering. *Int. J. Biol. Macromol.* **2015**, *80*, 481–488.

(19) Chen, C.; Li, H.; Pan, J.; Yan, Z.; Yao, Z.; Fan, W.; Guo, C. Biodegradable composite scaffolds of bioactive glass/chitosan/carboxymethyl cellulose for hemostatic and bone regeneration. *Biotechnol. Lett.* **2015**, *37*, 457–465.

(20) Manjubala, I.; Basu, P.; Narendrakumar, U. In situ synthesis of hydroxyapatite/carboxymethyl cellulose composites for bone regeneration applications. *Colloid Polym. Sci.* **2018**, 1729–1737.

- (21) Raucci, M.; Alvarez-Perez, M.; Demitri, C.; Giugliano, D.; De Benedictis, V.; Sannino, A.; Ambrosio, L. Effect of citric acid crosslinking cellulose-based hydrogels on osteogenic differentiation. *J. Biomed. Mater. Res., Part A* **2015**, *103*, 2045–2056.
- (22) Teti, G.; Salvatore, V.; Focaroli, S.; Durante, S.; Mazzotti, A.; Dicarolo, M.; Mattioli-Belmonte, M.; Orsini, G. In vitro osteogenic and odontogenic differentiation of human dental pulp stem cells seeded on carboxymethyl cellulose-hydroxyapatite hybrid hydrogel. *Front. Physiol.* **2015**, *6*, No. 297.
- (23) Clarke, S.; Hoskins, N.; Jordan, G.; Henderson, S.; Marsh, D. In vitro testing of Advanced JAX Bone Void Filler System: species differences in the response of bone marrow stromal cells to  $\beta$  tricalcium phosphate and carboxymethylcellulose gel. *J. Mater. Sci.: Mater. Med.* **2007**, *18*, 2283–2290.
- (24) Garai, S.; Sinha, A. Biomimetic nanocomposites of carboxymethyl cellulose–hydroxyapatite: Novel three dimensional load bearing bone grafts. *Colloids Surf., B* **2014**, *115*, 182–190.
- (25) Sayed, M.; El-Maghraby, H.; Bondioli, F.; Naga, S. 3D Carboxymethyl Cellulose/Hydroxyapatite (CMC/HA) Scaffold Composites Based on Recycled Eggshell. *J. Appl. Pharm. Sci.* **2018**, *8*, 023–030.
- (26) Pasqui, D.; Torricelli, P.; De Cagna, M.; Fini, M.; Barbucci, R. Carboxymethyl cellulose–hydroxyapatite hybrid hydrogel as a composite material for bone tissue engineering applications. *J. Biomed. Mater. Res., Part A* **2014**, *102*, 1568–1579.
- (27) Zakharov, N.; Ezhova, Z. A.; Koval, E. M.; Kalinnikov, V.; Chalykh, A. Hydroxyapatite-carboxymethyl cellulose nanocomposite biomaterial. *Inorg. Mater.* **2005**, *41*, 509–515.
- (28) Feng, H.; Zhang, L.; Zhu, C. Genipin crosslinked ethyl cellulose–chitosan complex microspheres for anti-tuberculosis delivery. *Colloids Surf., B* **2013**, *103*, 530–537.
- (29) Haugh, M. G.; Murphy, C. M.; O'Brien, F. J. Novel freeze-drying methods to produce a range of collagen–glycosaminoglycan scaffolds with tailored mean pore sizes. *Tissue Eng., Part C* **2010**, *16*, 887–894.
- (30) Zhou, J.; Chang, C.; Zhang, R.; Zhang, L. Hydrogels prepared from unsubstituted cellulose in NaOH/urea aqueous solution. *Macromol. Biosci.* **2007**, *7*, 804–809.
- (31) Modulevsky, D. J.; Lefebvre, C.; Haase, K.; Al-Rekabi, Z.; Pelling, A. E. Apple derived cellulose scaffolds for 3D mammalian cell culture. *PLoS One* **2014**, *9*, No. e97835.
- (32) Olsson, E.; Hedenqvist, M. S.; Johansson, C.; Järnström, L. Influence of citric acid and curing on moisture sorption, diffusion and permeability of starch films. *Carbohydr. Polym.* **2013**, *94*, 765–772.
- (33) Stone, S. A.; Gosavi, P.; Athauda, T. J.; Ozer, R. R. In situ citric acid crosslinking of alginate/polyvinyl alcohol electrospun nanofibers. *Mater. Lett.* **2013**, *112*, 32–35.
- (34) Kim, H.-L.; Jung, G.-Y.; Yoon, J.-H.; Han, J.-S.; Park, Y.-J.; Kim, D.-G.; Zhang, M.; Kim, D.-J. Preparation and characterization of nano-sized hydroxyapatite/alginate/chitosan composite scaffolds for bone tissue engineering. *Mater. Sci. Eng., C* **2015**, *54*, 20–25.
- (35) Zhang, Q.; Lu, H.; Kawazoe, N.; Chen, G. Pore size effect of collagen scaffolds on cartilage regeneration. *Acta Biomater.* **2014**, *10*, 2005–2013.
- (36) Guex, A. G.; Puetzer, J. L.; Armgarth, A.; Littmann, E.; Stavrinidou, E.; Giannelis, E. P.; Malliaras, G. G.; Stevens, M. M. Highly porous scaffolds of PEDOT: PSS for bone tissue engineering. *Acta Biomater.* **2017**, *62*, 91–101.
- (37) Peter, M.; Binulal, N.; Soumya, S.; Nair, S.; Furuike, T.; Tamura, H.; Jayakumar, R. Nanocomposite scaffolds of bioactive glass ceramic nanoparticles disseminated chitosan matrix for tissue engineering applications. *Carbohydr. Polym.* **2010**, *79*, 284–289.
- (38) Neufurth, M.; Wang, X.; Schröder, H. C.; Feng, Q.; Diehl-Seifert, B.; Ziebart, T.; Steffen, R.; Wang, S.; Müller, W. E. Engineering a morphogenetically active hydrogel for bioprinting of bioartificial tissue derived from human osteoblast-like SaOS-2 cells. *Biomaterials* **2014**, *35*, 8810–8819.
- (39) Wang, X.; Tolba, E.; Schröder, H. C.; Neufurth, M.; Feng, Q.; Diehl-Seifert, B.; Müller, W. E. Effect of bioglass on growth and biomineralization of SaOS-2 cells in hydrogel after 3D cell bioprinting. *PLoS One* **2014**, *9*, No. e112497.
- (40) Gutiérrez-Hernández, J. M.; Escobar-García, D. M.; Escalante, A.; Flores, H.; González, F. J.; Gatenholm, P.; Toriz, G. In vitro evaluation of osteoblastic cells on bacterial cellulose modified with multi-walled carbon nanotubes as scaffold for bone regeneration. *Mater. Sci. Eng., C* **2017**, *75*, 445–453.
- (41) Sittichokechaiwut, A.; Edwards, J.; Scutt, A.; Reilly, G. Short bouts of mechanical loading are as effective as dexamethasone at inducing matrix production by human bone marrow mesenchymal stem cell. *Eur. Cells Mater.* **2010**, *20*, 45.
- (42) Manjubala, I.; Woesz, A.; Pilz, C.; Rumpler, M.; Fratzl-Zelman, N.; Roschger, P.; Stampfl, J.; Fratzl, P. Biomimetic mineral-organic composite scaffolds with controlled internal architecture. *J. Mater. Sci.: Mater. Med.* **2005**, *16*, 1111–1119.
- (43) Shafiee, A.; Seyedjafari, E.; Soleimani, M.; Ahmadbeigi, N.; Dinarvand, P.; Ghaemi, N. A comparison between osteogenic differentiation of human unrestricted somatic stem cells and mesenchymal stem cells from bone marrow and adipose tissue. *Biotechnol. Lett.* **2011**, *33*, 1257–1264.
- (44) Wang, H.; Zhi, W.; Lu, X.; Li, X.; Duan, K.; Duan, R.; Mu, Y.; Weng, J. Comparative studies on ectopic bone formation in porous hydroxyapatite scaffolds with complementary pore structures. *Acta Biomater.* **2013**, *9*, 8413–8421.
- (45) Yu, Z.; Xiao, C.; Huang, Y.; Chen, M.; Wei, W.; Yang, X.; Zhou, H.; Bi, X.; Lu, L.; Ruan, J.; Fan, X. Enhanced bioactivity and osteoinductivity of carboxymethyl chitosan/nanohydroxyapatite/graphene oxide nanocomposites. *RSC Adv.* **2018**, *8*, 17860–17877.
- (46) Modulevsky, D. J.; Cuerrier, C. M.; Pelling, A. E. Biocompatibility of subcutaneously implanted plant-derived cellulose biomaterials. *PLoS One* **2016**, *11*, No. e0157894.
- (47) Quan, R.; Zheng, X.; Xu, S.; Zhang, L.; Yang, D. Gelatin-chondroitin-6-sulfate-hyaluronic acid scaffold seeded with vascular endothelial growth factor 165 modified hair follicle stem cells as a three-dimensional skin substitute. *Stem Cell Res. Ther.* **2014**, *5*, No. 118.
- (48) Karageorgiou, V.; Kaplan, D. Porosity of 3D biomaterial scaffolds and osteogenesis. *Biomaterials* **2005**, *26*, 5474–5491.
- (49) Deng, Y.; Jiang, C.; Li, C.; Li, T.; Peng, M.; Wang, J.; Dai, K. 3D printed scaffolds of calcium silicate-doped  $\beta$ -TCP synergize with co-cultured endothelial and stromal cells to promote vascularization and bone formation. *Sci. Rep.* **2017**, *7*, No. 5588.
- (50) Shi, Q.; Li, Y.; Sun, J.; Zhang, H.; Chen, L.; Chen, B.; Yang, H.; Wang, Z. The osteogenesis of bacterial cellulose scaffold loaded with bone morphogenetic protein-2. *Biomaterials* **2012**, *33*, 6644–6649.